DOI: 10.48011/asba.v2i1.1531

# A Robust Digital Control of a Gyroscope with an Implicit Derivative Estimator

**Mateus Mussi Brugnolli** * **Gabriel Pereira das Neves** *
**Leonardo de P. Carvalho** * **Oswaldo Luiz do Valle Costa** *
**Bruno Augusto Angélico** *

* *Department of Telecommunications and Control Engineering, Escola Politécnica da USP, São Paulo, SP, Brazil (e-mails: (mateus_mmb, gabriel.pereira.neves, carvalho.lp)@usp.br, (oswaldo, angelico)@lac.usp.br).*

**Abstract:** Recently, a new state-space representation has been developed for output feedback control design. With this transformation, many mechanical systems can be represented with the system output measurements as the full state vector. Therefore, these models allow the design of output feedback controllers using state feedback gains. For this work, a set of uncertain models for a Control Moment Gyroscope is assembled and a polytope discretization is performed. The resulting set of models is transformed into the Implicit Derivative Estimator and integrators are added for the output tracking. Finally, a robust $\mathcal{H}_2$ digital control is designed, considering the set of uncertain models. The controller is validated through simulation and practical experiments.

*Keywords:* Robust control applications, Output feedback control (linear case), Robust control (linear case), Observers for linear systems, Uncertainty descriptions.

## 1. INTRODUCTION

The attitude control of satellites and spacecrafts are mostly developed using gyroscopic control systems. The Control Moment Gyroscope (CMG) is an example of an under-actuated system that can be implemented for the desired attitude control (Theis et al. (2014)). The ECP model 750 has four rotating gimbals which only the inner two are motorized. Through the conservation of angular momentum and the gyroscopic torque, the inner motors can rotate the outer gimbals, that have higher inertia.

Furthermore, the CMG allows the setup for many control theories. As examples, the linear model can be decoupled using the control theory (Angélico et al. (2017)), as well as nonlinear controllers (Toriumi and Angélico (2018)) and linear parameter varying (LPV) control were applied to the CMG (Theis et al. (2014)).

The implementation of linear controllers can be performed generally in three distinct methods. Firstly, a state feedback control is assumed and the derivative states that are not measured can be estimated through approximations, for example using the Euler backward formula. Alternatively, the same state feedback scheme is assumed and the states are estimated using observers (Peaucelle and Ebihara (2014); Gao et al. (2017). Lastly, an output feedback control can be designed (Rosa et al. (2018)).

Recently, Angélico et al. (2019) developed a new state-space model representation called as implicit derivative estimator. This method has properties of the three methods previously mentioned. After a transformation of the state-space considering that the derivative states are estimated, the state observation is implicit within the linear model. Therefore, a state feedback control can be designed, given that all states will be output measurements. Essentially, such state feedback is also an output feedback control.

This paper main contributions are (i) defining a set of continuous models of the CMG that have the disc angular speed as uncertainty; (ii) discretization of the previous polytope; (iii) application of the implicit derivative estimator for the CMG model; (iv) a robust digital control design that considers the model uncertainties; (v) the validation of the controller through practical experiments.

The notation is standard. The function diag($x$) makes a diagonal matrix of zeroes except the main diagonal with the elements of a vector $x$; Trace($X$) is the sum of elements on the main diagonal of a matrix $X$, and $He(G)$ represents the sum of $G$ with its conjugate matrix.

This work is organized as follows: in Section 2, the CMG modeling is described and a set of uncertain models is assembled. Next, Section 3 a robust $\mathcal{H}_2$ control is designed considering the set of uncertainties. The controller is validated through simulations and practical experiments in Section 4. Lastly, some final statements are addressed in Section 5.

## 2. CMG MODELING

The CMG model 750 from ECP Company is a nonlinear system with four degrees of freedom. The diagram of the Fig. 1 shows four rigid bodies that rotate around their

⋆ This work was supported by Fundação de Amparo à Pesquisa do Estado de São Paulo (FAPESP), grant 2017/22130-4 and Coordenação de Aperfeiçoamento de Pessoal de Nível Superior - Brazil (CAPES) - Finance Code 001.

respective rotation axes (#1,#2,#3,#4), which defines the four degrees of freedom: $\theta_1, \theta_2, \theta_3, \theta_4$.

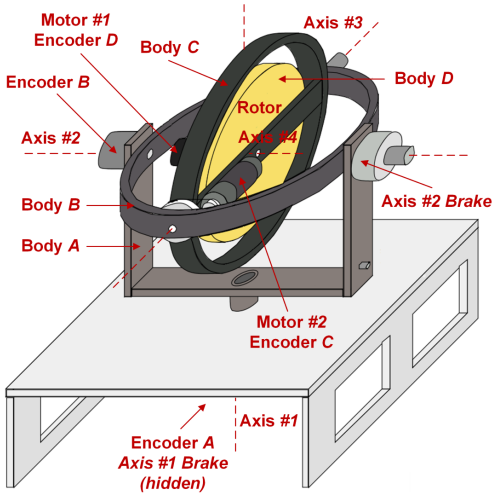


Fig. 1. Control Moment Gyroscope Diagram (Toriumi and Angélico (2018)).

There are two actuators in the system: a DC motor attached in axis #3, that applies a torque $T_2$ into the Body C and directly changes the angular position $\theta_3$; and a DC motor attached in the axis #4, that produces a torque $T_1$ into Body D (also known as disc) and affects directly $\theta_4$. Note that rotation of bodies A and B are free of actively applied torques. The movement of Body B is due to the conservation of angular momentum and Body A rotates due to the gyroscopic torque (Toriumi et al. (2018)).

The system sensors are four incremental encoders that provide the measurement of the four degrees of freedom. The general control objective of the CMG system is to track reference signals for positions $\theta_1$ and $\theta_2$ through the torques $T_1$ and $T_2$. Since there are no angular velocity sensors ($\omega_n$), these variables must be estimated with derivative approximations or computed using states observers, e.g. the Kalman Filter.

The four nonlinear equations of the CMG are the same presented in the previous papers (Toriumi et al. (2018); Toriumi and Angélico (2018)). The Equations (1) to (4) express all dynamics of the four degrees of freedom, applying the two DC motor torques $T_1$ and $T_2$ and considering a viscous friction $\mu_n\omega_n$ on each axis $\#n$. Due to the limitation of space, the expression of each function $f_n$ is omitted.

$$T_1 - \mu_4\omega_4 + f_4(\theta_2, \theta_3, \omega_1, \omega_2, \omega_3, \dot{\omega}_1, \dot{\omega}_2, \dot{\omega}_4) = 0, \quad (1)$$

$$T_2 - \mu_3\omega_3 + f_3(\theta_2, \theta_3, \omega_1, \omega_2, \omega_4, \dot{\omega}_1, \dot{\omega}_3) = 0, \quad (2)$$

$$-\mu_2\omega_2 + f_2(\theta_2, \theta_3, \omega_1, \omega_2, \omega_3, \omega_4, \dot{\omega}_1, \dot{\omega}_2, \dot{\omega}_4) = 0, \quad (3)$$

$$-\mu_1\omega_1 + f_1(\theta_2, \theta_3, \omega_1, \omega_2, \omega_3, \omega_4, \dot{\omega}_1, \dot{\omega}_2, \dot{\omega}_3, \dot{\omega}_4) = 0. \quad (4)$$

To obtain linear models for the CMG, the dynamic solution of the acceleration on each angular position must be linearized in a control operation point. Furthermore, in the literature the most frequent state vector [1] is related to the angles $\theta_1$ and $\theta_2$ and the angular velocities $\omega_1, \omega_2$ and $\omega_3$, $x = [\theta_1 \ \theta_2 \ \omega_1 \ \omega_2 \ \omega_3]^T$.

[1] If the angle $\theta_3$ is included in the state space, the resulting model is not controllable.

One interesting feature of the CMG is that depending on the operating point, there are structural dynamic changes in the linear model. For example, linearizing in $x = [0 \ 0 \ 0 \ 0 \ 0]^T$ and $\theta_3 = 0$, the linear model is decoupled. Choosing negative $\theta_3$ as operation point, the linear model has minimum phase and it is coupled. However, choosing positive $\theta_3$ gives a linear model with a non-minimum phase and it is coupled as well.

For the sake of simplicity, this work only considers the decoupled condition ($\theta_3 = 0$), $\theta_1 = 0$ and $\theta_2 = 0$. At an operating point with $T_1 = 0$ and $T_2 = 0$, the continuous state-space model is represented in (5).

$$\begin{bmatrix} \omega_1(t) \\ \omega_2(t) \\ \dot{\omega}_1(t) \\ \dot{\omega}_2(t) \\ \dot{\omega}_3(t) \end{bmatrix} = \begin{bmatrix} 0 & 0 & 1 & 0 & 0 \\ 0 & 0 & 0 & 1 & 0 \\ 0 & 0 & -0.0203 & 0 & -0.1345\omega_4 \\ 0 & 0 & 0 & -0.0592 & 0 \\ 0 & 0 & 1.5301\omega_4 & 0 & -0.4338 \end{bmatrix} \begin{bmatrix} \theta_1(t) \\ \theta_2(t) \\ \omega_1(t) \\ \omega_2(t) \\ \omega_3(t) \end{bmatrix} + \begin{bmatrix} 0 & 0 \\ 0 & 0 \\ 0 & 0 \\ -38.5071 & 0 \\ 0 & 408.1947 \end{bmatrix} \begin{bmatrix} T_1(t) \\ T_2(t) \end{bmatrix}. \quad (5)$$

### 2.1 Linear Uncertainty Description

Foremost, the linear model in (5) is controllable, noting that angle $\theta_3$ is not a state. Using the decoupled model, the dynamic changes between minimum and non-minimum phase models do not interfere with the control design.

Usually, the linear control design for the CMG assumes that the $\omega_4$ remains close to a nominal value during the experiment. However, any variation of the torque $T_1$ surely changes the angular velocity $\omega_4$. Therefore, a set of linear models that considers the $\omega_4$ as system uncertainty is applied for this work. The control design must track the desired output signals considering a range of $\omega_4$.

Subsequently, a range or even a grid of values for $\omega_4$ must be chosen. The CMG Manual states that the nominal value for $\omega_4$ is 400 rpm, with minimum value 200 rpm and maximum value 800 rpm, for safety purposes. For this work, a range of $\omega_4$ from 300 rpm to 500 rpm was assumed. This range was chosen due to the observation of past control experiments of the CMG.

The continuous linear model in (5) is specified in each limit of the range of $\omega_4$, obtaining two continuous state spaces. However, the focus of this work is the application of digital control, therefore the linear models must be discrete. The main issue is that even though two continuous models are convex, their discrete counterparts are not necessarily convex. The discretization of uncertain models still is a challenge and with few methods available in the literature (Shieh et al. (1998); de Souza and Trofino (2006); Hetel et al. (2007); Braga et al. (2013)).

Herein, the procedure presented in Braga et al. (2013) was implemented. Such discretization scheme is based on Taylor series expansions, considering polytopic uncertainties in the continuous-time system (Equation (5)), assuming that the sampling period $T_s$ is constant. Using the same notation of Braga et al. (2013), consider that the state space of Equation (5) has the structure of Equation (6), transforming the uncertainty of $\omega_4$ into a simplex $\alpha$.

$$\dot{x}(t) = E(\alpha)x(t) + F(\alpha)u(t) \tag{6}$$

The state-space matrices for the discrete-time system obtained via the procedure are in the form of homogeneous polynomials of the degree $\ell$. These polynomials represent uncertain parameters, which are norm bounded and also are a set in the unit simplex. Hence, the system obtained via the procedure can be written as

$$A(\alpha) = A_\ell(\alpha) + \Delta A_\ell(\alpha); B(\alpha) = B_\ell(\alpha) + \Delta B_\ell(\alpha). \tag{7}$$

Note that the additional terms in Equation (7), matrices with "$\Delta$" representing the residue of approximation, depends on the number of terms Taylor series expansion. Each matrix in (7) is obtained as

$$A_\ell(\alpha) = \sum_{j=0}^{\ell} \frac{E(\alpha)^j}{j!} {T_s}^j, \tag{8}$$

$$B_\ell(\alpha) = \sum_{j=0}^{\ell} \frac{E(\alpha)^{j-1}}{j!} {T_s}^j F(\alpha), \tag{9}$$

$$\Delta A_\ell(\alpha) = e^{E(\alpha)T_s} - A_\ell(\alpha), \tag{10}$$

$$\Delta B_\ell(\alpha) = (\int_0^{T_s} e^{E(\alpha)s} ds) F(\alpha) - B_\ell(\alpha). \tag{11}$$

*Remark*: It is important to point out that to guarantee the system performance it is necessary to bound the system norm. A way to cope with this issue is to use the Small Gain Theorem for this task (Zhou and Doyle (1998)). Another important aspect is that as the degree $\ell$ increases, the residue of approximation norm decreases. Therefore, if the Small Gain Theorem criterion is not satisfied with a given $\ell$, a direct solution is to increase the degree $\ell$ until the performance criterion is satisfied.

The discretization of the system model presented in (5) had a fixed sampling period of $T_s = 0.025$ seconds and the Taylor series was expanded with $\ell = 2$, which satisfied the performance criterion. The resulting set $(A_\ell(\alpha), B_\ell(\alpha))$ was convex and appropriate for robust digital control design.

### *2.2 Implicit Derivative Estimator State-Space*

The implicit derivative estimator state-space is a non-minimal representation which all states are measurements of the outputs of the system (Angélico et al., 2019). The requirement is that original discrete state-space must have a set of positions and their respective velocities as the state vector, a common feature of mechanic systems. Note that the current discrete state vector is $x[n] = [\theta_1[n]\ \theta_2[n]\ \omega_1[n]\ \omega_2[n]\ \omega_3[n]]^T$.

As a possible solution, each discrete model is augmented to include $\theta_3$ and creating a new state vector $x_d[n] = [\theta_1[n]\ \theta_2[n]\ \theta_3[n]\ \omega_1[n]\ \omega_2[n]\ \omega_3[n]]^T$. Basically, in the third row and column of $A_\ell(\alpha)$ and in the third row of $B_\ell(\alpha)$ an appropriate number of zeros is inserted, not modifying any dynamic of the model. Notice that the resulting model is not controllable, however, another transformation will be applied. Generally, the resulting state-space has the block-matrices of Equation (12). Also, note that the matrices can be dependent on the parameter $\alpha$ of a simplex $\Lambda$.

$$\begin{bmatrix}\Theta[n+1]\\ \Omega[n+1]\end{bmatrix} = \left[\begin{array}{c|c} A_{11}(\alpha) & A_{12}(\alpha) \\ \hline A_{21}(\alpha) & A_{22}(\alpha)\end{array}\right] \begin{bmatrix}\Theta[n]\\ \Omega[n]\end{bmatrix} + \begin{bmatrix}B_1(\alpha)\\ B_2(\alpha)\end{bmatrix} u[n]. \tag{12}$$

The main feature of the implicit derivative estimator model comes with the approximation of the derivative states, for example, a First-Order Euler backward for each $\Omega[n]$. Accordingly, the resulting model is presented in (13).

$$\begin{bmatrix}\Theta[n+1]\\ \frac{1}{T_s}(\Theta[n+1]-\Theta[n])\end{bmatrix} = \left[\begin{array}{c|c} A_{11}(\alpha) & A_{12}(\alpha) \\ \hline A_{21}(\alpha) & A_{22}(\alpha)\end{array}\right] \begin{bmatrix}\Theta[n]\\ \frac{1}{T_s}(\Theta[n]-\Theta[n-1])\end{bmatrix} + \begin{bmatrix}B_1(\alpha)\\ B_2(\alpha)\end{bmatrix} u[n] \tag{13}$$

Therefore, two expressions are obtained:

$$\Theta[n+1] = \left(A_{11}(\alpha) + \frac{A_{12}(\alpha)}{T_s}\right)\Theta[n] \cdots - \frac{A_{12}(\alpha)}{T_s}\Theta[n-1] + B_1(\alpha)u[n], \tag{14}$$

$$\frac{\Theta[n+1]-\Theta[n]}{T_s} = \left(A_{21}(\alpha) + \frac{A_{22}(\alpha)}{T_s}\right)\Theta[n] \cdots - \frac{A_{22}(\alpha)}{T_s}\Theta[n-1] + B_2(\alpha)u[n]. \tag{15}$$

Adding the dynamics of (14) and (15), the implicit derivative estimator model representation is expressed in (16). Note that $\Theta[n] = [\theta_1[n]\ \theta_2[n]\ \theta_3[n]]^T$ and $\Omega[n] = [\omega_1[n]\ \omega_2[n]\ \omega_3[n]]^T$ for the CMG and all states are measurements of the system outputs.

$$\begin{bmatrix}\Theta[n+1]\\ \Theta[n]\end{bmatrix} = \begin{bmatrix}P_1(\alpha) & P_2(\alpha)\\ I & 0\end{bmatrix}\begin{bmatrix}\Theta[n]\\ \Theta[n-1]\end{bmatrix} + \begin{bmatrix}P_3(\alpha)\\ 0\end{bmatrix} u[n], \tag{16}$$

$$P_1(\alpha) = \frac{1}{1+T_s}\left(T_s A_{11}(\alpha) + A_{12}(\alpha) \cdots + T_s A_{21}(\alpha) + A_{22}(\alpha) + I\right),$$

$$P_2(\alpha) = \frac{-1}{1+T_s}\left(A_{12}(\alpha) + A_{22}(\alpha)\right),$$

$$P_3(\alpha) = \frac{T_s}{1+T_s}\left(B_1(\alpha) + B_2(\alpha)\right).$$

An interesting remark is that the state space in (16) is controllable and observable. The controllability is recovered since the state space internally computes the angular velocity $\omega_3[n]$ from the measurements of $\theta_3[n]$ and $\theta_3[n-1]$. In Table 1, the parameters are each model are shown, recalling that the Taylor degree was $\ell = 2$, thus the discretization created a polynomial with the same degree.

Furthermore, each model was augmented with integrators to track set-point positions for $\theta_1[n]$ and $\theta_2[n]$, as presented in Fig. 2. Note that $(A_d, B_d)$ are obtained from Equation (16) and are dependent on $\alpha$. The augmented system has two additional states $v[n]$, resulting in a new state vector $x'[n] = [x[n]\ v[n]]^\top$.

The augmented system matrices are represented as

$$A'_d(\alpha) = \begin{bmatrix}A_d(\alpha) & 0\\ -C & I\end{bmatrix}, \quad B'_d(\alpha) = \begin{bmatrix}B_d(\alpha)\\ 0\end{bmatrix},$$

Table 1. Implicit Derivative Estimator Model Parameters

| | $P_1$ | | | $P_2$ | | | $P_3$ | |
|---|---|---|---|---|---|---|---|---|
| $\alpha_1^2$ | 1.83 | 0 | −0.17 | −0.83 | 0 | 0.17 | 0 | −0.02 |
| | 0 | 2.00 | 0 | 0 | −1.00 | 0 | −0.02 | 0 |
| | 1.94 | 0 | 1.77 | −1.94 | 0 | −0.79 | 0 | 0.25 |
| $\alpha_1\alpha_2$ | 2.82 | 0 | −0.28 | −1.79 | 0 | 0.28 | 0 | −0.04 |
| | 0 | 3.02 | 0 | 0 | −2.00 | 0 | −0.05 | 0 |
| | 3.11 | 0 | 2.70 | −3.11 | 0 | −1.72 | 0 | 0.50 |
| $\alpha_2^2$ | 1.94 | 0 | −0.10 | −0.94 | 0 | 0.10 | 0 | −0.01 |
| | 0 | 2.00 | 0 | 0 | −1.00 | 0 | −0.02 | 0 |
| | 1.16 | 0 | 1.88 | −1.17 | 0 | −0.90 | 0 | 0.25 |

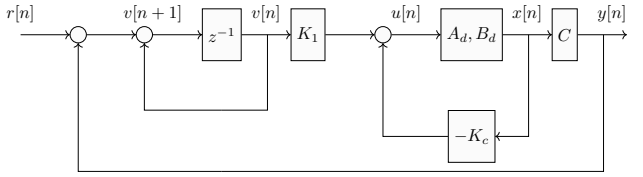


Fig. 2. Discrete time state feedback with integrator.

and $C_d' = [C\ 0]$, while the control is $K' = [K_C\ -K_I]$.

*Remark*: The implicit derivative estimator transformation was applied to each model, however, one must assure that the set of models remains convex. Due to the limitation of space, two proof sketches are briefly addressed. First, if the sampling period $T_s$ is small enough, the derivative approximation becomes most similar to the real values. Therefore, the implicit derivative estimator does not change the system dynamics and it is considered as a basis transformation. Alternatively, one may increase the degree of the approximation as much as possible. Thus, similar to the previous method, the derivative approximation draws near to the original value and the transformation only changes the basis. The key aspect of these proof sketches is to check the model eigenvalues to guarantee the properties of a basis transformation.

## 3. ROBUST CONTROL DESIGN

As discussed in Section 2, a discrete convex set of models for the CMG was assembled, considering the disc velocity $\omega_4$ as uncertainty. Accordingly, robust digital control is designed with a set of uncertain models. The design is described by Lemma 1 (de Oliveira et al. (1999)), considering a state-space represented by (17), where $w[n]$ is an exogenous input and $z[n]$ is the controlled output.

$$\begin{aligned} x'[n+1] &= (A_d'(\alpha) - B_d'(\alpha)K')x'[n] + B_w w[n] \\ z[n] &= (C_z - D_{zu}K')x'[n] \end{aligned} \quad (17)$$

*Lemma 1.* There exists a controller for the model in (17) satisfying the constraints $\|H(z)\|_2^2 < \mu$ if there exist symmetric matrices $W_\ell(\alpha)$ and $X$, and matrices $G$ and $Z$ of compatible dimensions satisfying the LMIs:

$$\text{Trace}(X) < \mu, \quad (18)$$

$$\begin{bmatrix} X & C_zG + D_{zu}Z \\ \star & He(G) - W_\ell(\alpha) \end{bmatrix} > 0, \quad (19)$$

$$\begin{bmatrix} W_\ell(\alpha) & A_d'(\alpha)G + B_d'(\alpha)Z & B_w \\ \star & He(G) - W_\ell(\alpha) & 0 \\ \star & \star & I \end{bmatrix} > 0, \quad (20)$$

and holds for all $\alpha \in \Lambda$. If a feasible solution is obtained, a robust controller is given by $K' = ZG^{-1}$.

The controller of Lemma 1 was designed using the YALMIP, the ROLMIP (Agulhari et al. (2019)) for creating the matrices $A_d'(\alpha)$, $B_d'(\alpha)$ and $W_\ell(\alpha)$ with degree $\ell = 2$ and the Semidefinite Programming was solved using the SeDuMi. The matrices $B_w, C_z$ and $D_{zu}$ were tuned to achieve the desired system performance for an exogenous input $w[n]$. The chosen matrices were:

$$B_w = I_8, C_z = \begin{bmatrix} C_{zp} \\ 0_{[8\times 8]} \end{bmatrix}, D_{zu} = \begin{bmatrix} 0_{[8\times 2]} \\ D_{zup} \end{bmatrix},$$

$$C_{zp} = \text{diag}\left(\begin{bmatrix} 1 & 1 & \frac{\sqrt{2}}{2} & 1 & 1 & 0.1 & \frac{\sqrt{2}}{20} & 0.1 \end{bmatrix}\right),$$

$$D_{zup} = \begin{bmatrix} \sqrt{5} & 0 & 0 & 0 & 0 & 0 & 0 & 0 \\ 0 & \sqrt{5} & 0 & 0 & 0 & 0 & 0 & 0 \end{bmatrix}^T.$$

Applying Lemma 1, the controller was designed, such that

$$K' = [-K_C\ K_I], K_I = \begin{bmatrix} 0 & -0.0365 \\ -0.0246 & 0 \end{bmatrix},$$

$$K_C = \begin{bmatrix} 0 & -9.7664 & 0 & 0 & 8.6782 & 0 \\ -2.3493 & 0 & 1.2220 & 1.7149 & 0 & -1.2893 \end{bmatrix}.$$

An important note is that the matrices $G$ and $Z$ did not have a fixed structure and the controller of Lemma 1 was decoupled. That occurred due to the decoupled linearization in Section 2.

## 4. SIMULATION AND PRACTICAL RESULTS

Foremost, the usual sampling period of experiments for the ECP 750 is lower than $T_s = 0.01$ seconds (Angélico et al. (2017)). However, the application of such fast sampling period presented poor performance using the model representation of the implicit derivative estimator. The reason is that using such a model designs a control signal that is sensitive to measurement variations in a short period.

The sensibility of the model of implicit derivative estimator is related to the chosen order of the approximation of the derivative and the noise present in the output measurements. Thus, a higher sampling period of $T_s = 0.025$ seconds reduced the sensibility of the output measurements and improved the control law performance, especially in practical experiments. To validate the controller of Lemma 1, a step response and a sinusoidal response were performed through simulations and practical experiments with the ECP model 750 [2].

The experiment setup starts with the positioning of the CMG in the decoupled position ($\theta_1 = 0, \theta_2 = 0, \theta_3 = 0$) that was the linearized position of the linear models. Next, with the breaks of $\theta_1$ and $\theta_2$ activated, a PI controller actuates motor #1 until it reaches the nominal speed of $\omega_4 = 400$ rpm. Finally, the breaks are released, the PI controller is turned off and the controller of Section 3 begins to track the output set-points.

[2] The readers are invited to see a quick video of the practical experiment through the link: https://youtu.be/oemUZ2KPZ-g

The step response is shown in Fig. 3 and 4, in which the system outputs $\theta_1$ and $\theta_2$ track a filtered step pulse, both for simulation and practical experiments. Although the model was linearized close to the origin, the performance of the static gain control using state feedback was investigated into a far operation point, up to 30°.

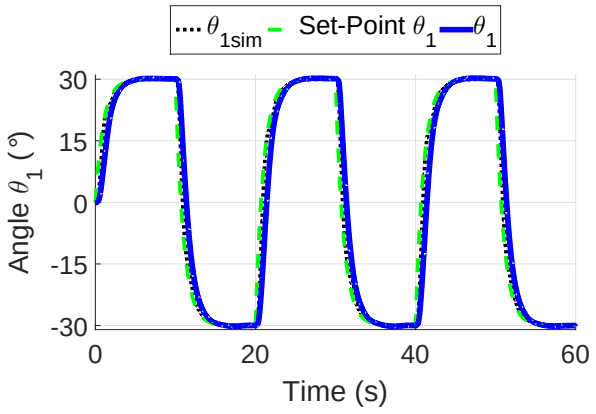


Fig. 3. Step Response: Output $\theta_1$.

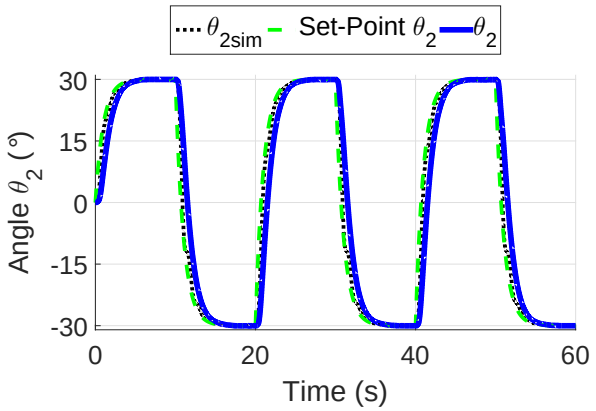


Fig. 4. Step Response: Output $\theta_2$.

The control signals $T_1$ and $T_2$ for the step response are shown in Fig. 5. It stands out that the torque $T_1$ of the practical experiment presented a distinct performance. Most likely, the reason is that the DC motor dynamics and Coulomb friction of the joints were not included in the model.

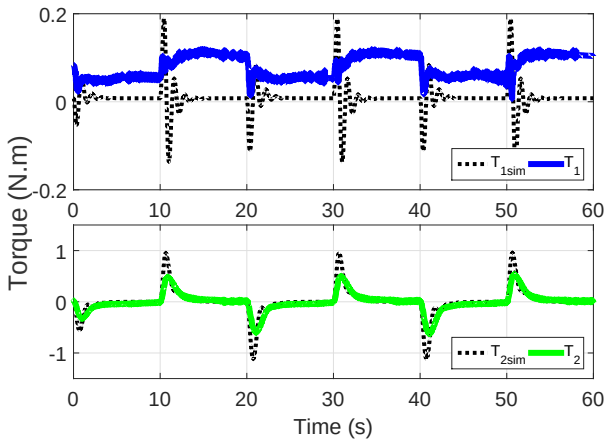


Fig. 5. Step Response: Control Signals $T_1, T_2$.

Ultimately, the disc angular speed is shown in Fig. 6. Remark that during the CMG modeling, the linear models considered that the $\omega_4$ was uncertain and within a range of 300 to 500 rpm. Fig. 6 shows that the disc angular speed maintained within the uncertainty of $\omega_4$, asserting the system stability with good performance for such range.

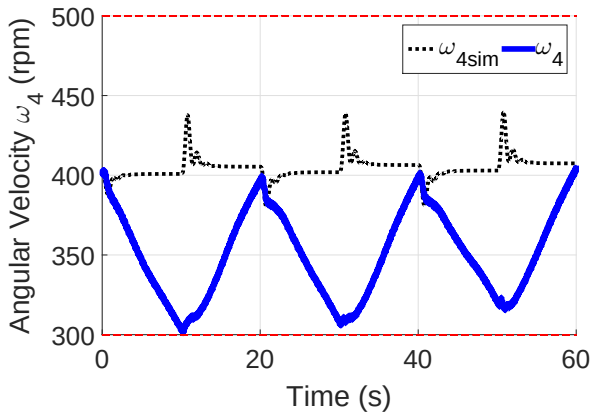


Fig. 6. Step Response: Disc Angular Speed $\omega_4$.

Next, the sinusoidal response is shown in Fig. 7 and 8. The amplitude was increased to 40°, with good performance considering that the controller is a static gain. Additionally, a small delay to the set-point was detectable.

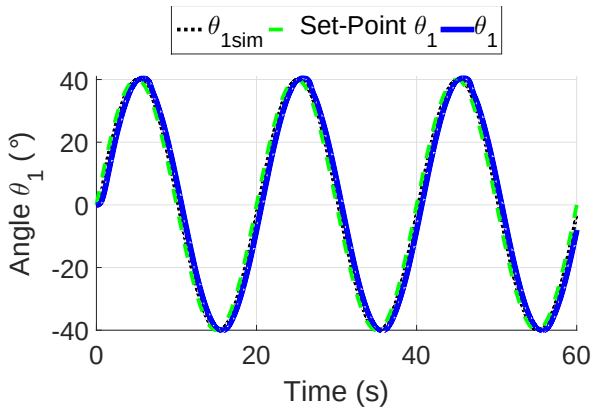


Fig. 7. Sinusoidal Response: Output $\theta_1$.

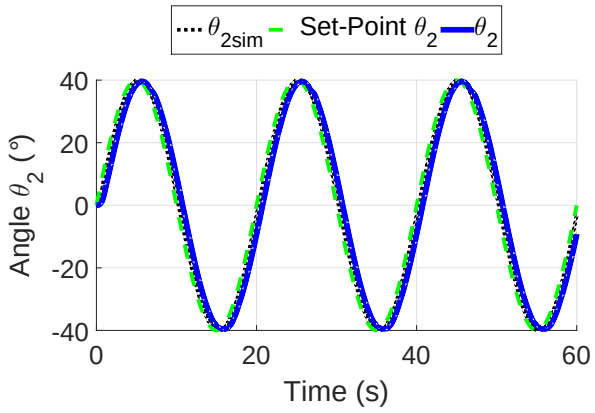


Fig. 8. Sinusoidal Response: Output $\theta_2$.

As previously, Fig. 9 presents the control signals $T_1$ and $T_2$. In such a case, it is evident the similarity of the torque $T_2$ between the simulation and the practical experiments.

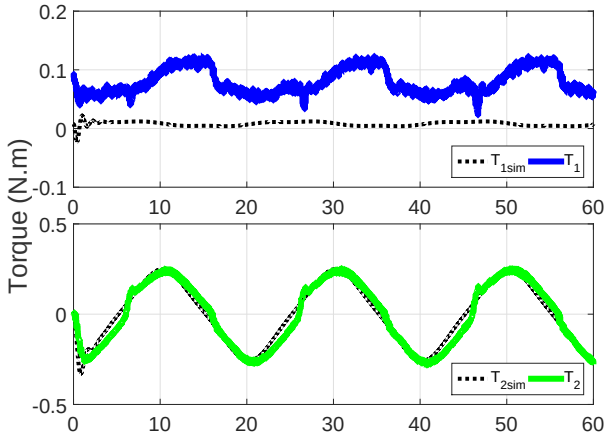


Fig. 9. Sinusoidal Response: Control Signals $T_1, T_2$.

The last results in Fig. 10 show that the disc angular speed $\omega_4$ remained within the range of 300 to 500 rpm assumed in Section 2, reasserting the system stability and control performance.

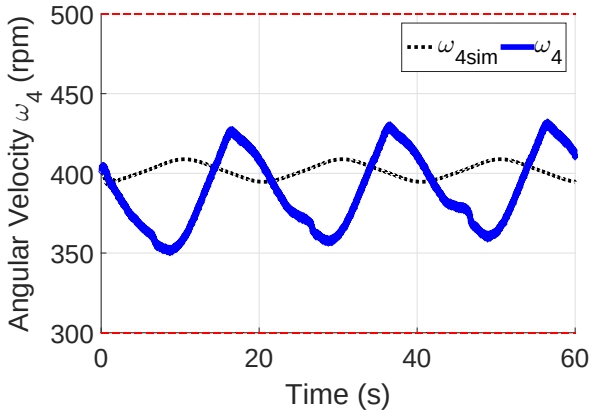


Fig. 10. Sinusoidal Response: Disc Angular Speed $\omega_4$.

## 5. CONCLUSIONS

A discrete polytope set for the CMG has been successfully assembled, considering that the disc angular speed is uncertain. Each model was transformed into the implicit derivative estimator representation, which allowed a design of output feedback using the structure of state feedback. The model states were the three system outputs measurements and integrators were added for the output tracking. The controller of Lemma 1 managed to track high amplitude set-points, considering that the control law was a static gain and operated away from the linearized point. Furthermore, the disc angular speed remained within the range defined in the model uncertainties.

## REFERENCES


Agulhari, C.M., Felipe, A., Oliveira, R.C.L.F., and Peres, P.L.D. (2019). Algorithm 998: The Robust LMI Parser — A toolbox to construct LMI conditions for uncertain systems. *ACM Transactions on Mathematical Software*, 45(3), 36:1–36:25.

Angélico, B.A., Brugnolli, M.M., and das Neves, G.P. (2019). Digital h-inf robust control of mechanical system with implicit observer. In *2019 IEEE 58th Conference on Decision and Control (CDC)*, 1171–1176.

Angélico, B.A., Toriumi, F.Y., Barbosa, F.D.S., and Das Neves, G.P. (2017). On guaranteeing convergence of discrete LQG/LTR when augmenting it with forward PI controllers. *IEEE Access*, 5, 27203–27210.

Angélico, B.A., Barbosa, F.S., and Toriumi, F.Y. (2017). State feedback decoupling control of a control moment gyroscope. *Journal of Control, Automation and Electrical Systems*, 28(1), 26–35.

Braga, M.F., Morais, C.F., Tognetti, E.S., Oliveira, R.C.L.F., and Peres, P.L.D. (2013). A new procedure for discretization and state feedback control of uncertain linear systems. In *52nd IEEE Conference on Decision and Control*, 6397–6402.

de Oliveira, M.C., Geromel, J.C., and Bernussou, J. (1999). An LMI optimization approach to multiobjective controller design for discrete-time systems. In *Proceedings of the 38th IEEE Conference on Decision and Control*, volume 4, 3611–3616 vol.4.

de Souza, C.E. and Trofino, A. (2006). Gain-scheduled $\mathcal{H}_2$ controller synthesis for linear parameter varying systems via parameter-dependent lyapunov functions. *International Journal of Robust and Nonlinear Control*, 16(5), 243–257.

Gao, N., Darouach, M., and Alma, M. (2017). $\mathcal{H}_\infty$ dynamic observer design for linear discrete-time systems. *IFAC-PapersOnLine*, 50(1), 2756 – 2761. 20th IFAC World Congress.

Hetel, L., Daafouz, J., and Iung, C. (2007). LMI control design for a class of exponential uncertain systems with application to network controlled switched systems. In *2007 American Control Conference*, 1401–1406.

Peaucelle, D. and Ebihara, Y. (2014). LMI results for robust control design of observer-based controllers, the discrete-time case with polytopic uncertainties. *IFAC Proceedings Volumes*, 47(3), 6527 – 6532. 19th IFAC World Congress.

Rosa, T.E., Morais, C.F., and Oliveira, R.C. (2018). New robust lmi synthesis conditions for mixed gain-scheduled reduced-order dof control of discrete-time lpv systems. *International Journal of Robust and Nonlinear Control*, 28(18), 6122–6145.

Shieh, L.S., Wang, W., and Chen, G. (1998). Discretization of cascaded continuous-time controllers and uncertain systems. *Circuits, Systems and Signal Processing*, 17(5), 591–611.

Theis, J., Radisch, C., and Werner, H. (2014). Self-scheduled control of a gyroscope. *IFAC Proceedings Volumes*, 47(3), 6129 – 6134. 19th IFAC World Congress.

Toriumi, F.Y., Angélico, B.A., and Tannuri, E.A. (2018). Feedback linearization approach applied to a control moment gyroscope with SISO configuration. In *2018 13th IEEE International Conference on Industry Applications (INDUSCON)*, 174–179.

Toriumi, F.Y. and Angélico, B.A. (2018). Robust nonlinear control applied to a control moment gyroscope with SISO configuration. *IFAC-PapersOnLine*, 51(25), 152 – 157. 9th IFAC Symposium on Robust Control Design ROCOND 2018.

Zhou, K. and Doyle, J.C. (1998). *Essentials of Robust Control*. Prentice-Hall.